

Preprint of article about an open hardware RTU device.

# Multiple Sensor Interface by the same hardware to USB and serial connection

David Nuno Quelhas \*

Preprint submitted to 'arXiv', February 8, 2022

## Abstract

The Multiple Sensor Interface is a simple sensor interface that works with USB, RS485 and GPIO. It allows one to make measurements using a variety of sensors based on the change of inductance, resistance, capacitance, and frequency using the same connector and same electronic interface circuit between the sensor and the microcontroller. The same device also provides some additional connectors for small voltage measurement. Any sensors used for the measurement of distinct phenomena can be used if the sensor output is based on inductance, resistance, capacitance or frequency within the measurement range of the device, obtaining a variable precision depending on the used sensor. The device presented is not meant for precise or accurate measurements. It is meant to be a reusable hardware that can be adapted/configured to a varied number of distinct situations, providing, to the user, more freedom in sensor selection as well as more options for device/system maintenance or reuse.

**Keywords:** Sensor systems and applications; Oscillators; Design aiming for reuse, repurpose, repair, customization.

---

## 1 Introduction

The electronic waste (e-waste) is a modern problem under increasing concern and awareness, there are various possible approaches to reduce and mitigate it, most obvious is the collection and recycling of discarded devices, however the most ideal was just to make technology that lasts because not only is physically fit by quality design, production, and components; but because its design was intended to be most versatile ensuring the same device can be used and reused in various applications/contexts just by changing connections, jumpers, and firmware configurations. Some design aspects for making a device more reusable are: use of standard connectors and protocols, think of it as a module to be part of a larger system, minimize barriers for connecting/interfaces components and devices from distinct manufacturers.

### 1.1 Project objectives and trade-offs

This article is focused on the design of a sensor interface device with USB and serial(UART,RS-485), aimed to allow interface to many distinct 2-wire sensors based on the change of inductance, resistance, capacitance, frequency, and also small voltage; sensors that can be interchanged using the same hardware and same port of the device, thus meaning the electronics designed must also be versatile.

Obviously providing a versatile device to the users will have its negative trade-offs, like:

- 1- probably significant lower precision/accuracy;
- 2- some sensor calibration must be provided/done by the end user after replacing a sensor;
- 3- the calibration function will not be linear or 'easy' as desired for sensors and its interfaces.

-However for some applications the mentioned trade-offs are not necessarily a deal-breaker, like when the user is technical and is ok with using a device that requires more setup/configuration, some users like devices that are more customizable or repairable. Also a device that if no longer useful for a user, it might still be useful for another user on a different application/context.

### 1.2 License and context

The hardware design here disclosed is distributed under "CERN Open Hardware Licence Version 2 - Weakly Reciprocal" (CERN-OHL-W), its associated software/firmware under GNU licenses (GPL, LGPL).

This article is published under the Creative Commons license CC BY-NC-SA 4.0 (Attribution-NonCommercial-ShareAlike 4.0 International).

This article is about a 'hobby' project done by the author (David Nuno Quelhas, MSc Electronics Eng, alumni of Instituto Superior Tecnico, Portugal) with occasional 'work' between years 2012 and 2021 on his 'free time'.

### 1.3 Prior art review

The topic and devices commonly described in literature as Multiple Sensor Interface and also as Universal Sensor Interface, commonly fall under 3 distinct categories: a) Device that has a more versatile interface or signal conditioning circuit capable of interfacing various sensor types; b) Device that includes various specialized interface or signal conditioning circuits for each sensor type, typically built using various PCB boards for the sensors, to connect or stack into a PCB board with a micro-processor that will register

---

\*Lisboa, Portugal; E-mail: david.n.quelhas@gmail.com  
<https://pt.linkedin.com/in/dquelhas>  
ORCID: 0000-0002-0282-0972  
<https://multiple-sensor-interface.blogspot.com>

and/or transmit the measurements, or alternatively have all these different circuits integrated inside a single integrated circuit (micro-chip); c) Hardware and/or software systems that collect or register sensor data from various distinct sensing devices/circuits, that may apply some processing to the raw data for obtaining measurements, then to be transmitted to other systems or to a data storage, and so these hardware/software systems may also be called/named 'interface'.

The article review presented here will be about 'more versatile interface or signal conditioning circuit' that is the category most similar to this article. Types of versatile sensor interface found on prior art:

1- Interfacing resistive or capacitive sensors by measuring the charge-discharge time of an RC circuit, or measuring the frequency or PWM from an oscillator whose pace is controlled by the speed of a capacitor charge-discharge trough a resistor. (S. N. Nihtianov et al. 2001)[6]; (J. Kwon, B. Jung, et al. 2011)[7]; (F.M.L.v.d. Goes and G.C.M. Meijer 1997)[8].

2- Interfacing sensors based on variation of impedance (includes sensor based on variation of resistance, capacitance or inductance) by an LCR meter, impedance meter or potentiostat circuit. (Xiaowen Liu et al. 2009)[9]; (Dumb-rava V., Svilainis L. 2007)[10]; (HIOKI website 2021)[11]; (Terrones M., Sun L. 2013)[12].

The Multiple Sensor Interface presented on this article has a working principle more similar to the circuits mentioned as type 1 (RC time or frequency or PWM of oscillator), however in comparison with the mentioned references/articles, the interface circuit of this article can interface more distinct sensor types, namely besides interfacing resistive and capacitive sensors it also interfaces inductive sensors and sensors by frequency measurement using exactly the same circuit and connector/port, also it is a simple circuit with a reduced number of components.

The Multiple Sensor Interface presented on this article in comparison to the circuits mentioned as type 2 (LCR or impedance meters), has the advantage of not requiring an AC voltage/signal generator for exciting the measurement circuit, and not requiring the complex hardware and/or complex post processing for digitizing voltage signal waveforms, that is typically required for the calculation of amplitude and

phase difference of voltage signals, on the measurement of impedance by LCR or impedance meters.

A comparison regarding the accuracy or precision of this sensor interface and other interfaces/devices was not made, since the stated focus of the article is how to achieve a most versatile sensor interface, and also considering that such comparison may be easier when considering specific type(s) of sensor/application.

## 2 Sensor Interface Device

Here is presented the Multiple Sensor Interface (Fig.1), the interface main components/sub-circuits are: The connectors and sensor interface circuits (oscillators) for inductance, resistance, capacitance and frequency (CH.0, CH.1); the connectors and over-voltage protection(zener diode) for frequency measurement (CH.2, CH.3, CH.4, CH.5); the connectors and interface circuit for voltage measurement (ADC.0, ADC.1, ADC.2, ADC.3); analog multiplexer for the sensor channels, the microprocessor(PIC18F2550); I2C EEPROM for storing calibration tables; USB connector; connector and circuit for RS-485 and UART; digital outputs connector (OUT.1, OUT.2).

The digital outputs have the value of a boolean function defined by the user, boolean functions with logic variables that are the result of a comparison ('bigger' or 'smaller than), between the value/measurement of a sensor channel and a configurable threshold value. The connectors used for frequency measurement may be connected to external single sensor interface circuits (oscillators).

### 2.1 The sensor interface circuit (oscillator)

The sensor interface (Fig.2) is an oscillator with a circuit design based on the Pierce oscillator with some modifications. The 1st difference is that there is no quartz crystal, and on the location of the crystal will be connected the sensor to be measured (variable inductance or resistance or capacitance), the 2nd difference is that instead of simple inverters ('NOT' gates) will be used Schmitt-trigger inverters(high-speed Si-gate CMOS, 74HC14), this is a very relevant difference that will allow the oscillator to work even with a resistive or capacitive sensor, in fact the interface circuit works with sensors mostly as a Schmitt-Trigger oscillator. Also the Schmitt-Trigger inverters may minimize signal jitter of

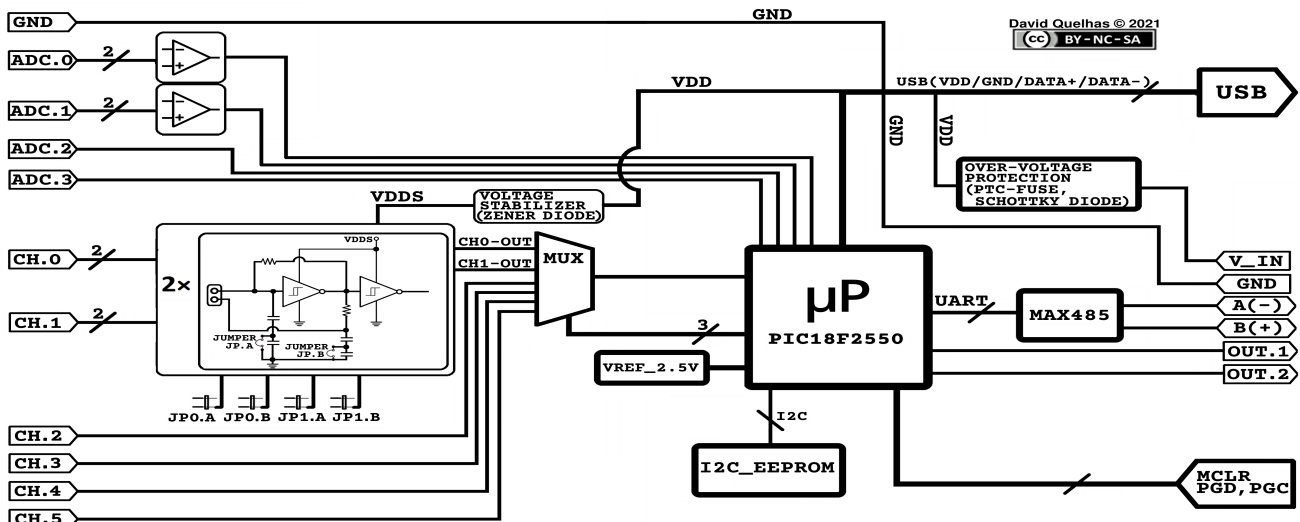


Figure 1: Diagram of the Multiple Sensor Interface device.

the oscillator output.

The sensor interface circuit has 2 pairs of series capacitors (C1 2.2nF,C1-A 22pF and C2 2.2nF,C2-B 22pF) instead of just 2 capacitors(C1,C2) so the value of C1 and C2 can be adjusted just by placing/removing a jumper; placing a jumper removes C1-A or C1-B from the circuit making 2.2nF the value of C1 or C2; removing the jumper lets the capacitors in series making 21.78pF the total value of (C1, C1-A) or (C2, C2-B). So on the rest of the article, whenever is mentioned C1 or C2 is meant the resulting capacitor value that can be 2.2nF(jumper on) or 21.78pF(jumper off), accordingly with mentioned jumper configuration.

The sensors can be connected directly on the Multiple-Sensor Interface(on then screw terminals/connectors), or by using a cable; for a cable longer than 20cm is recommended the use of shielded twisted-pair(STP) cable to prevent cross-talk between sensor channels or external EMI.

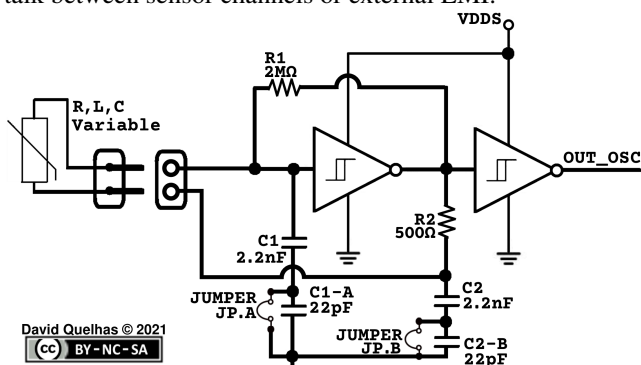


Figure 2: Schematic of the sensor interface circuit (oscillator).

### 3 Measurement process

The Multiple-Sensor device has a microprocessor (PIC18F2550) that is able to make frequency and voltage measurements, so the device makes frequency measurements for sensor channels CH.0 to CH.5 ; and makes voltage measurements for sensor channels ADC.0 to ADC.3; these frequency and voltage measurements made by the device are designated as the RAW\_value of a sensor channel. To obtain the measurement of a sensor channel the device uses a 2 column calibration table that is a long list of points (RAW\_value; measurement) relating the measurement value (obtained during calibration by an external reference device) to the corresponding RAW\_value obtained on the Multiple-Sensor device, these calibration tables are stored on an I2C EEPROM memory on the Multiple-Sensor device.

The Multiple-Sensor device can work in two modes: single-channel or multiple-channel, the CH.0 to CH.5 RAW\_value(frequency) are calculated through a counter/timer of the PIC18F2550 by periodically reading its value and calculating the frequency  $f = \text{count} / \text{period}$  ( $[\text{Hz}] = [\text{cycles}] / [\text{s}]$ ). So in single-channel mode the frequency is always calculated on the selected/enabled sensor channel, in multiple-sensor mode the frequency is calculated for each sensor channel sequentially (time-division multiplexing), since there are 6 channels to measure but only on counter/timer of the microprocessor for that job. Thus in multiple-channel mode a measurement takes 6x more time to be updated/refreshed than in single-channel mode.

For the sensor channels ADC.0 to ADC.3 the RAW\_value

is the voltage of those channels measured by using the ADC (Analog to Digital Converter) of the microprocessor and also reading a 2.5V voltage reference.

The sensor measurements are calculated by searching the RAW\_value on the correspondent calibration table, and by using from the table 2 points (RAW\_value,measurement) referenced here as points P and Q such that the measured RAW\_value is bigger than RAW\_value of P and is lower than RAW\_value of Q; then is calculated a linear equation:  $\text{measurement} = a \cdot (\text{RAW\_value}) + b$ , defined by the points P and Q. So every-time the device calculates a sensor measurement, it will calculate the correspondent linear equation for the current RAW\_value and use it to obtain the current measurement (Fig.3) .

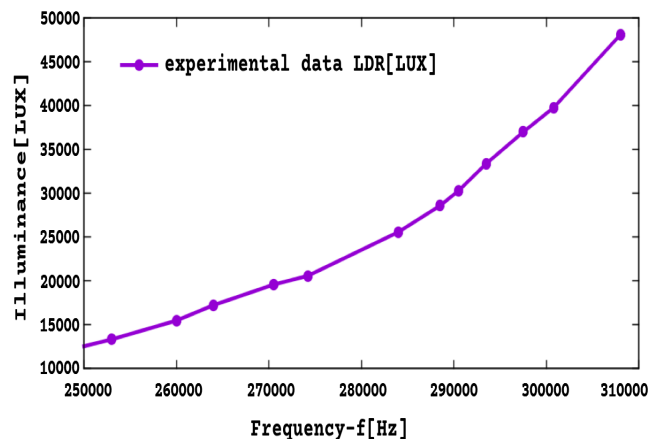


Figure 3: Plot experimental data with line, LDR light(brightness) sensor connected on Multiple-Sensor Interface; example of a calibration table exclusively from experimental data.

#### 3.1 Device calibration for a sensor

Device calibration is about obtaining calibration tables for each sensor channel, here are 2 ways to obtain a calibration table:

1- Do a full manual calibration using an external meter as reference where both the reference meter and the Multiple-sensor device(with a sensor connected) are exposed to same stimulus/environment that is controllable by the user to produce all adequate variations/intensities necessary to record an extensive calibration table, with all experimental pairs of (RAW\_value,measurement).

2- Using a know function that relates the measured phenomena to the obtained RAW\_value on the Multiple-Sensor device (obtained by theoretical or experimental study), although a purely theoretical calibration could be used, probably is better or easier to obtain a calibration table by using a known function and have its constants/parameters calculated by a data fitting to some few experimental data points (RAW\_value, measurement) obtained for the device calibration. So for example if the know function had 6 constants/parameters you would require at least 6 different experimental measurements to obtain the function for that sensor channel, then having the function is just a question calculating a longer list of pairs (RAW\_value,measurement) on the desired measurement range. The (Fig.4) is the result of fitting the model function  $\text{Illuminance}(f) = (a + (b/(c + d \cdot f))) \cdot ((n \cdot f^2) + m)$ , to the points (229Hz, 0LUX; 8500Hz, 10LUX; 14000Hz, 30LUX; 76500Hz, 300LUX; 130000Hz, 1072LUX; 194000Hz, 3950LUX).

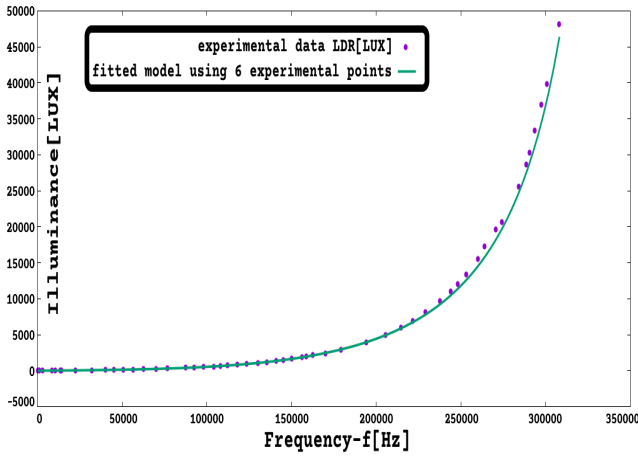


Figure 4: Plot experimental data and fitted model (by using 6 points), LDR light (brightness) sensor connected on Multiple-Sensor Interface.

#### 4 Sensor Interface Circuit Analysis

##### 4.1 Multiple-Sensor Interface for Inductive sensors

When is connected an inductor or inductive sensor the Multiple-Sensor Interface (Fig.2) may work as a Pierce Oscillator (where the sensor is connected instead of a quartz crystal). The theoretical analysis used here for the oscillator was based on a model of 2 circuit blocks named 'A' and 'β' connected for feedback by connecting the output of one to the input other. The 'A' is an electronic amplifier providing voltage gain, the 'β' is an electronic filter providing frequency selection (resonance), so whatever voltage signal amplified by 'A' is frequency selected by 'β' and feed back to the input of A for further amplification. As know this oscillator is start-up by whatever noise ( $v_s$ ) available at the input of 'A', Fig.5 is a diagram depicting this concept.

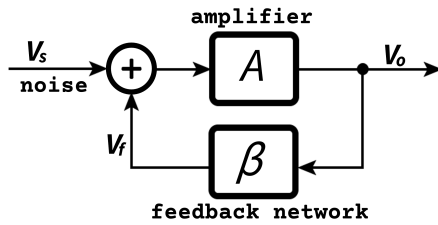


Figure 5: Diagram of model for the oscillator with an inductive sensor (Pierce Oscillator, model of feedback linear oscillator).

The analysis of the circuit as Pierce oscillator was made using the Barkhausen stability criterion, that says  $A\beta = 1$  to be possible to occur sustained oscillations (oscillations on steady state analysis). The purpose/focus is to obtain the inductance (of sensor) as function of oscillation frequency, although most of the circuit analysis strategy used here is similar as for typical Pierce Oscillator with piezoelectric crystal, as available on the bibliography list "Crystal Oscillators for Digital Electronics" class notes by Peter McLean [2]. So from  $A\beta=1$  results:  $|A\beta|=1$  and  $\angle A\beta = \pm n2\pi$ . This mathematical expression simply says that a circuit with a feedback loop after reaching the steady-state is expected that any voltage signal (for example  $V_o$ ) will remain steady.

Starting the analysis on Fig.6, using a possible representation of Fig.5 diagram with the 'feedback network' represented by its hybrid parameters (2-port network h-parameters). (Jaeger, R.C., Blalock T.N., 2011)[1], (Peter McLean, 2020)[2]

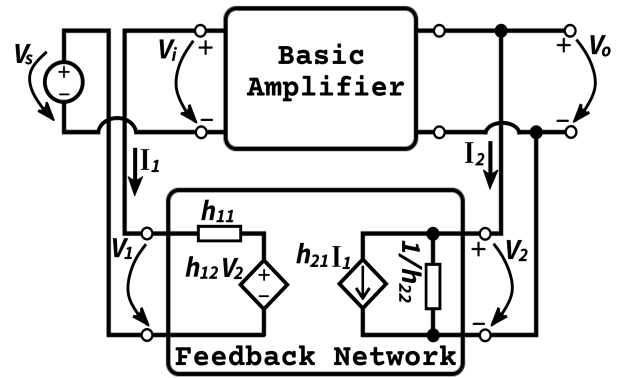


Figure 6: Representation of oscillator circuit by the h-parameters for feedback circuit (Pierce oscillator).

The Schmitt-Trigger inverter and resistors  $R_1, R_2$  belong to block 'A', the capacitors  $C_1, C_2$ , and inductive sensor  $L_s$  belong to block 'β'.

Since the 'Basic Amplifier' has a very big input resistance the current  $I_1$  will be very small (the electric current on the input of the inverter, CMOS 'NOT' gate, is negligible), so by using the h-parameters to represent the feedback circuit block is possible to make the following simplifications/approximations: 1- The current source  $h_{21}I_1$  is also negligible (equal to zero, so removed from circuit); 2- The voltage drop across component  $h_{11}$  is negligible (since  $V_{11} = h_{11}I_1, I_1 \rightarrow 0 \Rightarrow V_{11} \rightarrow 0$ ) and so  $h_{11}$  can be relocated to inside the circuit block 'A' keeping  $V_i$  as the name for the voltage drop on the input of 'A' block; 3- The  $1/h_{22}$  can be relocated to inside the circuit block 'A' since is connected in parallel to the input of 'β' block that is also the output of 'A' block. (Peter McLean, 2020)[2]

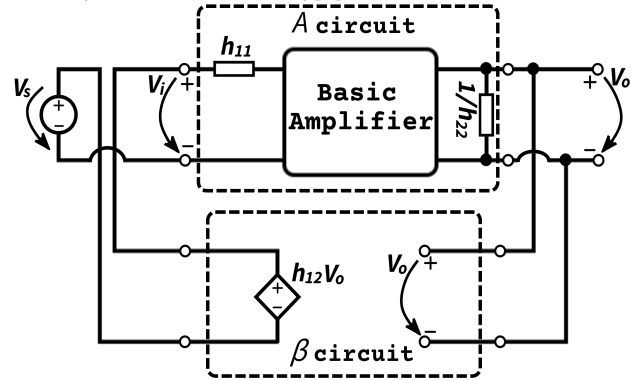


Figure 7: Simplified representation of oscillator circuit (Pierce osc.)

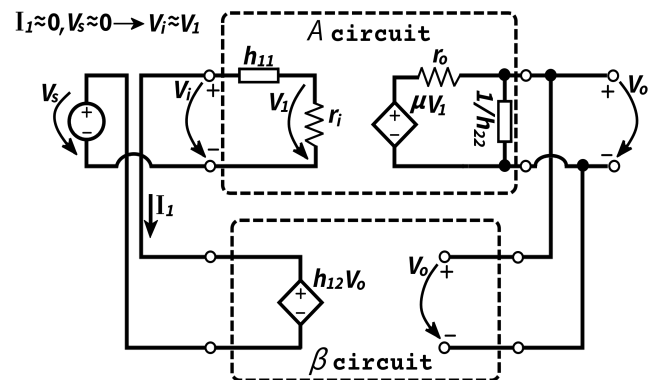


Figure 8: More simplified representation of the circuit (Pierce osc.)

The block 'Basic Amplifier' is then replaced by its Thevenin equivalent circuit, obtaining Fig.8 circuit. From this is obtained the transfer function (Laplace transform) of 'A' block ( $V_o = AV_i, 1/h_{22} = h_{22}^{-1}$ ) and 'β' block ( $V_1 = \beta V_2$ ):

$$A = \frac{h_{22}^{-1}}{h_{22}^{-1} + r_o} \mu \frac{r_i}{r_i + h_{11}} \quad \beta = h_{12}$$

The feedback network (the same network displayed on Fig.6 represented by h-parameters) is the frequency-selecting  $\pi$ (shaped)-network on Fig.9, where  $Z_1$ ,  $Z_2$ ,  $Z_s$  are respectively  $C_1, C_2, L_{sensor}$  of the Multiple Sensor Interface with an inductive sensor (Pierce oscillator).

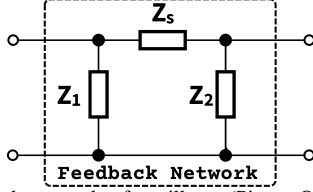


Figure 9: Feedback network of oscillator (Pierce Oscillator, Multiple-Sensor Interface with inductive sensor).

Based on the circuit of the feedback network and using the definitions of h-parameters of a 2-port network are obtained the values:

$$h_{11} = Z_1 || Z_s \quad h_{22}^{-1} = Z_2 || (Z_1 + Z_s) \quad h_{12} = \frac{Z_1}{Z_1 + Z_s}$$

(where  $||$  is the impedance of 2 components in parallel,  $Z_1 || Z_s = (Z_1 Z_s) / (Z_1 + Z_s)$ ;  $h_{11} = (V_1 / I_1) |_{V_2=0}$ ;  $h_{12} = (V_1 / V_2) |_{I_1=0}$ ;  $h_{22} = (I_2 / V_2) |_{I_1=0}$ ). (Jaeger, R.C., Blalock T.N., 2011)[1])

Finally:

$$A = \frac{Z_2 || (Z_1 + Z_s)}{Z_2 || (Z_1 + Z_s) + r_o} \mu \frac{r_i}{r_i + (Z_1 || Z_s)} \quad \beta = \frac{Z_1}{Z_1 + Z_s}$$

In the circuit of Pierce oscillator (Fig.2) the amplifier was made by a gate inverter (CMOS 'NOT' gate) and a feedback resistor ( $R_1=2M\Omega$ ), biasing the inverter and allowing it to function as a high-gain inverting amplifier. The input resistance of CMOS 'NOT' gate is very large and so making the approximation  $r_i = +\infty$  the expression of 'A' is significantly simplified, So obtaining: (Peter McLean 2020)[2]

$$A\beta = \left( \frac{Z_2 || (Z_1 + Z_s)}{Z_2 || (Z_1 + Z_s) + r_o} \mu \right) \left( \frac{Z_1}{Z_1 + Z_s} \right) = \frac{Z_1 Z_2 \mu}{Z_2 (Z_1 + Z_s) + r_o (Z_1 + Z_2 + Z_s)} \quad (1)$$

If  $Z_1$ ,  $Z_2$ ,  $Z_s$  are purely reactive impedances given by  $Z_1 = jX_1$ ,  $Z_2 = jX_2$ ,  $Z_s = jX_s$  ( $j = \sqrt{-1}$ ), then (1) becomes:

$$A\beta = \frac{X_1 X_2 \mu}{X_2 (X_1 + X_s) - j r_o (X_1 + X_2 + X_s)} \quad (2)$$

The Barkhausen criterion states  $A\beta=1 \rightarrow \angle A\beta = \pm n2\pi$ , this means the phase shift of the loop 'A $\beta$ ' must be zero, and so that implies that the imaginary part of (2) must be zero. That is, for stable oscillations on the circuit of Fig.6 with a Feedback Network of Fig.9, it must be assured: (Peter McLean 2020)[2]

$$X_1(\omega_0) + X_2(\omega_0) + X_s(\omega_0) = 0 \quad (3)$$

At the frequency  $\omega_0$  (frequency of oscillation at steady state), using (3) with (2), is obtained: (Peter McLean 2020)[2]

$$A(\omega_0)\beta(\omega_0) = -\mu \frac{X_1(\omega_0)}{X_2(\omega_0)} \quad (4)$$

To start the oscillations the loop gain must be greater than unity (during Transient Response), but after achieving the Steady State Response on the Pierce oscillator for oscillations to occur the loop gain  $A(\omega_0)\beta(\omega_0)$  of (4) must be equal to '1'(unity). Since the amplifier is an inverter ('NOT' gate with  $R_1$  feedback resistor) then  $\mu$  is a negative number, and so  $X_1(\omega_0)$  and  $X_2(\omega_0)$  must have the same sign (both positive or negative).

Thus, if  $Z_1(\omega_0)$  is capacitive ( $X_1(\omega_0) = -1/(\omega_0 C_1)$ ), then by (4)  $Z_2(\omega_0)$  must also be capacitive ( $X_2(\omega_0) = -1/(\omega_0 C_2)$ ). (Peter McLean 2020)[2]

Considering this and using (3) its possible to conclude that  $Z_s(\omega_0)$  must be inductive since  $X_s(\omega_0) = -X_1(\omega_0) - X_2(\omega_0)$ , this is if  $X_1(\omega_0)$  and  $X_2(\omega_0)$  are negative numbers then  $X_s(\omega_0)$  must be a positive number, then  $X_s = \omega_0 L_s$ .

So having  $C_1$ ,  $C_2$ ,  $L_s$  on the feedback network (where  $L_s$  is the component representing the inductive sensor on the Multipl-Sensor Interface) the (3) becomes:

$$-\frac{1}{\omega_0 C_1} - \frac{1}{\omega_0 C_2} + \omega_0 L_s = 0 \quad (5)$$

So defining "load capacitance"  $C_L$  as: (Peter McLean 2020) [2]

$$\frac{1}{C_L} = \frac{1}{C_1} + \frac{1}{C_2} \quad (6)$$

The frequency of oscilation on the Pierce oscillator (using  $C_1$ ,  $C_2$ ,  $L_s$ ) is:

$$\omega_0 = \frac{1}{\sqrt{L_s C_L}} \Leftrightarrow f_0 = \frac{1}{2\pi \sqrt{L_s C_L}} \quad (7)$$

So the expression (theoretical) of measured inductance  $L_{sensor}$  as a function of frequency(f) is:

$$L_{sensor} = L_s = \frac{1}{4\pi^2 C_L f^2} = \frac{C_1 + C_2}{4\pi^2 C_1 C_2 f^2} \quad (8)$$

On experimental tests done was observed that when using  $C_1=C_2=2.2nF$  (JP.A and JP.B closed) or when using  $C_1=21.78pF$  (JP.A open),  $C_2=2.2nF$  (JP.B closed), with decreasing values of  $L_s$  connected, the oscillation frequency exhibited a sudden change, at some small value of L(around  $10\mu H$  for  $C_1=C_2=2.2nF$ ), not coherent with theoretical model of Pierce oscillator. This may be related to the fact the same circuit also implements a Schmitt-Trigger oscillator(next section), that oscillates under different criteria, so the author opinion is when  $L_s$  approaches some small value it may change from Pierce oscillator to Schmitt-Trigger oscillator. Fig.10 and Fig.11 shows the experimental data for various inductance values connected as the sensor and the plot  $L_s(f)$  using (8) with  $C_1=C_2=2.2nF$  and  $C_1=21.78pF$ ,  $C_2=2.2nF$ .

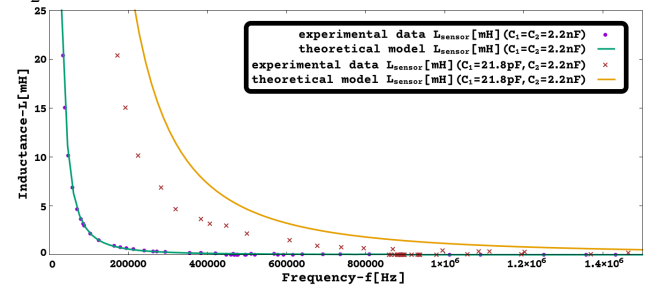


Figure 10:  $L_s(f)$ [mH]([Hz]) with  $C_1=C_2=2.2nF$  and  $C_1=21.78pF$ ,  $C_2=2.2nF$  (Pierce Osc., Multi-Sensor Int. with inductive sensor)

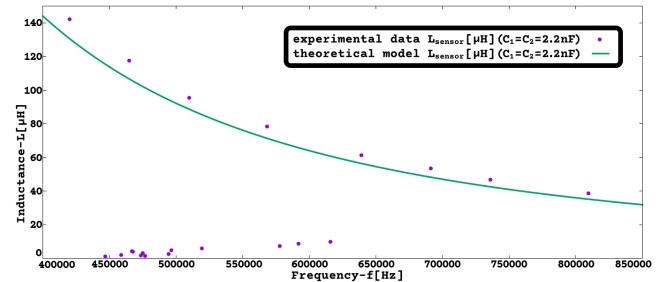


Figure 11: Frequency jump of  $L_s(f)$ [ $\mu H$ ]([Hz]) with  $C_1=C_2=2.2nF$  (Pierce Osc., Multi-Sensor Int. with inductive sensor).

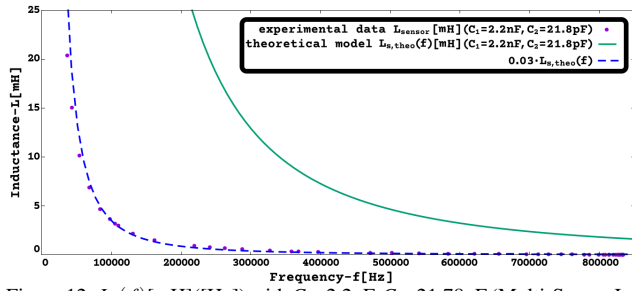


Figure 12:  $L_s(f)$  [mH] ([Hz]) with  $C_1=2.2\text{nF}$ ,  $C_2=21.78\text{pF}$  (Multi-Sensor Int. with inductive sensor).

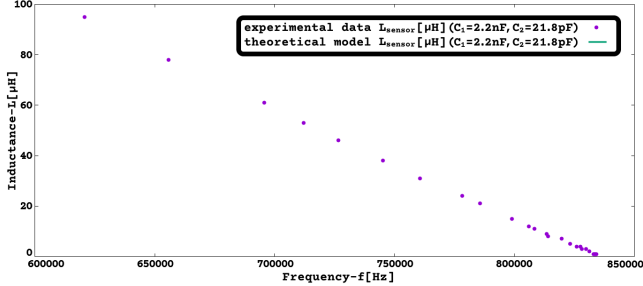


Figure 13: Experimental data of  $L_s$  in  $[0\mu\text{H}; 100\mu\text{H}]$ , with  $C_1=2.2\text{nF}$ ,  $C_2=21.78\text{pF}$  (Multi-Sensor Int. with inductive sensor).

Since the mentioned sudden change of oscillator mode and frequency is not adequate on a  $L_s(f)$  function usable for sensor interfacing; then on experimental tests with jumper configuration: JP.A on and JP.B off ( $C_1=2.2\text{nF}$ ,  $C_2=21.78\text{pF}$ ), it was observed a continuous and progressive  $f(L_s)$  function. With  $C_1=2.2\text{nF}$ ,  $C_2=21.78\text{pF}$ , the experimental  $L_{s,expr}(f)$  followed a straight line for  $L_s$  in  $[0\mu\text{H}; 100\mu\text{H}]$ , then for  $L_s > 100\mu\text{H}$  the experimental  $L_{s,expr}(f)$  continued with a shape that has some visual similarity to theoretical (as Pierce oscillator), but with significantly different  $L_s$  values. It was noticed that for larger values of  $L_s$  the theoretical (Pierce oscillator, JP.A on, JP.B off) could be approximated to the experimental data by a constant multiplicative factor ( $L_{s,expr}(f) \approx 0.03 \cdot L_{s,theo}(f)$ ), for  $L_s > 1\text{mH}$ ), as visible in Fig. 12 and Fig. 13.

For modeling(data fitting) purposes, the author knows that a function  $L_s(f)=(a+(b/(c+d \cdot f)) \cdot (n \cdot f + m))$ , where 'a,b,c,d,m,n' are constants to fit, can be fitted to experimental data on both low and high values of  $L_s$ .

On following section 5 was used an approximated model (for Schmitt-Trigger oscillator) applied to Multiple-Sensor Interface with inductive sensor (JP.A on, JP.B off), that exhibited a theoretical  $L_s(f)$  plot much closer to the experimental data, corroborating the hypothesis that with jumper configuration JP.A on, JP.B off ( $C_1=2.2\text{nF}$ ,  $C_2=21.78\text{pF}$ ), it operates as a Schmitt-Trigger oscillator, where  $L_s$  acts as an impedance influencing  $C_1$  charge and discharge speed.

#### 4.2 Multiple-Sensor Interface for Resistive sensors

In case you connect a resistive sensor (or capacitive) to the Multiple-Sensor Interface it will not be able to satisfy the conditions for oscillation of equations (3) and (4), consequent of the Barkhausen criterion applied to the circuit, as it was explained on the previous section that on the  $\pi$ (shaped)-network of Fig.9 if  $Z_1$  and  $Z_2$  are capacitive (corresponding to  $C_1$  and  $C_2$ ) then  $Z_s$  must be inductive so that  $A(\omega_0)\beta(\omega_0)=1$ . So the conclusion is when you connect a resistive sensor (or capacitive) you no longer have a Pierce Oscillator. The Multiple-Sensor Interface is made

using Schmitt-trigger inverters (high-speed Si-gate CMOS, 74HC14), and the Schmitt trigger is a bistable multivibrator that can be used to implement another type of multivibrator, the relaxation oscillator. So in the case of a resistive sensor the circuit to analyze is a Schmitt-trigger inverter connected to a network of resistors and capacitors.

To analyze this circuit the Schmitt-Trigger inverter was replaced by a theoretical switch that changes the voltage of node  $v_o$  to VDD5 (power supply stabilized voltage for the sensor interface) when voltage  $v_i$  is lower than  $V_T^-$ , and changes  $v_o$  to GND when voltage  $v_i$  is higher than  $V_T^+$ .

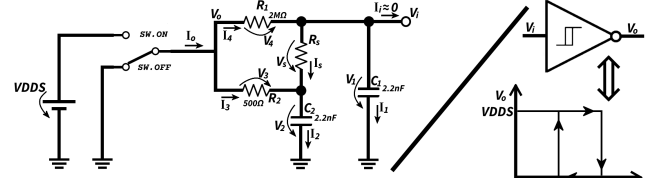


Figure 14: Multi-Sensor Int., resistive sensor (Schmitt-trigger osc.)

- So the circuit of Fig.14 was analyzed to obtain  $f(R_s)$ , and then its inverse function  $R_s(f)=R_{s,sensor}$  that may be useful for using/configuring the Multiple-Sensor Interface. Notice that  $i_i \approx 0$  since  $v_i$  is the input of a Schmitt-trigger inverter (high-speed Si-gate CMOS) that has a very high input impedance and so  $i_i \approx 0$  is an appropriate approximation simplifying the circuit. So from the circuit are obtained the equations:

$$\begin{aligned} \text{Nodes and loops: } \quad & i_4 = i_s + i_1, & i_3 + i_s &= i_2, \\ & i_o = i_3 + i_4, & i_1 + i_2 &= i_o, & i_1 + i_2 &= i_3 + i_4, & v_1 - v_2 - v_s &= 0, \\ & v_4 + v_s + v_2 - v_o &= 0, & v_4 + v_s - v_3 &= 0, & v_3 &= v_o - v_2, \\ & v_4 = v_o - v_i, & v_2 &= v_i - v_s. \end{aligned}$$

$$\begin{aligned} \text{Components: } \quad & i_1 = C_1(dv_1/dt), & i_2 &= C_2(dv_2/dt), \\ & v_3 = R_2 i_3, & v_4 &= R_1 i_4, & v_s &= R_s i_s \end{aligned}$$

Solving:

$$\frac{v_o - v_i}{R_1} = \frac{v_s}{R_s} + C_1 \frac{dv_i}{dt} \quad (9)$$

$$\frac{v_o - v_i + v_s}{R_2} + \frac{v_s}{R_s} = C_2 \frac{dv_2}{dt} \quad (10)$$

$$\text{Solving: } v_2 = v_i - v_s \Rightarrow dv_2/dt = d(v_i - v_s)/dt \Rightarrow dv_2/dt = (dv_i/dt) - (dv_s/dt)$$

So using the previous result the (10) can be changed to:

$$\frac{v_o - v_i}{R_2} + \left( \frac{1}{R_2} + \frac{1}{R_s} \right) v_s = C_2 \left( \frac{dv_i}{dt} - \frac{dv_s}{dt} \right) \quad (11)$$

Solving (9) for  $v_s$  is obtained:

$$v_s = \frac{R_s(v_o - v_i)}{R_1} - R_s C_1 \frac{dv_i}{dt} \quad (12)$$

Calculating the derivative on both sides of (12) is obtained (remember  $v_o$  is a constant equal to VDD5 or GND depending on the position of the switch 'SW'):

$$\frac{dv_s}{dt} = \frac{-R_s}{R_1} \frac{dv_i}{dt} - R_s C_1 \frac{d^2 v_i}{dt^2} \quad (13)$$

Now using (12) and (13) to remove the variables  $v_s$  and  $dv_s/dt$  from equation (11) is obtained an equation solvable for determining  $v_i(t)$ :

$$\begin{aligned} \left( \frac{1}{R_2} + \frac{R_s}{R_2 R_1} + \frac{1}{R_1} \right) (v_o - v_i) = \\ \left( C_1 \left( 1 + \frac{R_s}{R_2} \right) + C_2 \left( 1 + \frac{R_s}{R_1} \right) \right) \frac{dv_i}{dt} + R_s C_1 C_2 \frac{d^2 v_i}{dt^2} \end{aligned} \quad (14)$$

The equation (14) is of the type:  $c(v_o - v_i) = b(dv_i/dt) + a(d^2 v_i/dt^2)$  that has the general solution:  $v_i(t) = v_o +$

$k_1 e^{\lambda_1 t} + k_2 e^{\lambda_2 t}$ , where  $k_1, k_2$  are integration constants to be defined by 'initial conditions' and  $\lambda_1, \lambda_2$  are defined by:  $a\lambda^2 + b\lambda + c = 0 \Leftrightarrow \lambda = \frac{-b \pm \sqrt{b^2 - 4ac}}{2a}$  and  $e$  is the Euler-Napier constant  $e = \sum_{n=0}^{\infty} (1/(n!))$ .

So for a solution to this circuit:  $a = R_s C_1 C_2$ ,  
 $b = (C_1(1 + (R_s/R_2))) + (C_2(1 + (R_s/R_1)))$ ,  
 $c = (1/R_2) + (R_s/(R_2 R_1)) + (1/R_1)$ .

Is selected the solution  $\lambda_2 = \frac{-b + \sqrt{b^2 - 4ac}}{2a}$  by setting  $k_1=0$ , because is the one that provides an adequate value for  $v_i(t)$ ,  $f(R_s)$ , consistent with experimental data, however for obtaining the function  $R_s(f)$  you may use any.

For convenience of making  $v_i(t)$  more similar to typical RC circuits is defined  $\tau = -1/\lambda$ , and so  $v_i(t) = v_o + k_2 e^{-t/\tau}$ .

Charging time of  $C_1$ :  $v_o = V_{DDS}$   
 $v_i(t=0) = V_T^- \rightarrow V_T^- = V_{DDS} + k_2 e^0 \rightarrow k_2 = V_T^- - V_{DDS}$   
 $v_i(t=T_C) = V_T^+ \rightarrow V_T^+ = V_{DDS} + k_2 e^{-T_C/\tau} \rightarrow$   
 $\rightarrow T_C = -\tau \ln((V_T^+ - V_{DDS})/(V_T^- - V_{DDS}))$

Discharging time of  $C_1$ :  $v_o = 0$   
 $v_i(t=0) = V_T^+ \rightarrow V_T^+ = 0 + k_2 e^0 \rightarrow k_2 = V_T^+$   
 $v_i(t=T_D) = V_T^- \rightarrow V_T^- = 0 + k_2 e^{-T_D/\tau} \rightarrow$   
 $\rightarrow T_D = -\tau \ln(V_T^-/V_T^+)$

The time for a complete cycle of charge and discharge of  $C_1$  is:  $T = T_C + T_D$ ; the frequency of  $v_i(t)$  is  $f = 1/T$ .

Solving:  $T = -\tau_2 \left( \ln \left( \frac{V_T^- - V_{DDS}}{V_T^+ - V_{DDS}} \right) + \ln \left( \frac{V_T^-}{V_T^+} \right) \right)$   
 $\Leftrightarrow T = \tau_2 \ln \left( \frac{(V_T^- - V_{DDS})V_T^+}{(V_T^+ - V_{DDS})V_T^-} \right)$

For convenience defining the constant 'H' by:  
 $H = \ln \left( \frac{(V_T^- - V_{DDS})V_T^+}{(V_T^+ - V_{DDS})V_T^-} \right)$ ,  
then  $f = 1/T \Leftrightarrow f = 1/(\tau_2 H) \Leftrightarrow f = -\lambda_2/H$ .

So the expression (theoretical) of measured resistance  $R_{sensor}$  as a function of frequency(f) is:

$$R_{sensor} = R_s = \frac{(C_1 + C_2)R_2 R_1 H f - R_2 - R_1}{(C_2 R_2 H f - 1)(C_1 R_1 H f - 1)} \quad (15)$$

Using the values  $C_1=C_2=2.2nF$ ,  $R_2=500\Omega$ ,  $R_1=2M\Omega$ ,  $V_T^-=1.2V$ ,  $V_T^+=2.2V$ ,  $V_{DDS}=4.18V$ , is obtained  $H=1.01496$ , Fig.15 shows experimental data for Multiple-Sensor Interface with various resistance values connected as the sensor and also shows the plot of  $R_{sensor}(f)$  using (15) with the mentioned values of  $C_1, C_2, R_2, R_1, H$ .

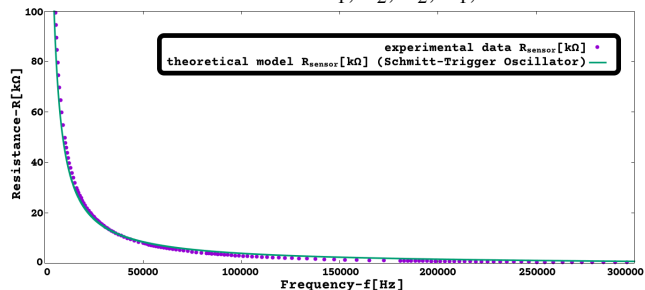


Figure 15:  $R_s$ [kΩ] versus frequency[0Hz, 300kHz] (Schmitt-Trigger Oscillator, Multiple-Sensor Interface with resistive sensor).

### 4.3 Multiple-Sensor Interface for capacitive sensors

In case you connect a capacitive sensor (or resistive) to the Multiple-Sensor Interface it will not be able to satisfy the conditions for oscillation of the Pierce oscillator, equations

(3) and (4), by  $A(\omega_0)\beta(\omega_0)=1$ , and so it is again a Schmitt-Trigger relaxation oscillator. So to analyze this circuit the Schmitt-trigger inverter was replaced by a theoretical switch (Schmitt-Trigger), just like previously with resistive sensors.

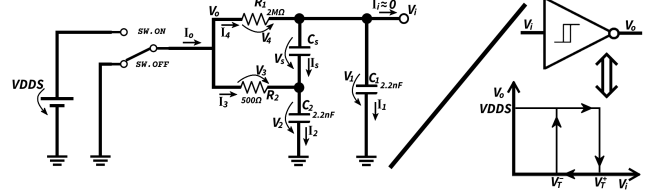


Figure 16: Multi-Sensor Int., capacitive sensor (Schmitt-trigger osc.)

So the circuit of Fig.16 was analyzed to obtain  $f(C_s)$ , and then its inverse function  $C_s(f)=C_{sensor}$  that is useful for using/configuring the Multiple-Sensor Interface. Notice that  $i_i \approx 0$  since  $v_i$  is the input of the Schmitt-trigger inverter (high-speed Si-gate CMOS) that has a very high input impedance and so  $i_i \approx 0$  is an appropriate approximation simplifying the circuit. So from the circuit are obtained the equations:

Nodes and loops:  $i_4 = i_s + i_1$ ,  $i_3 + i_s = i_2$ ,  
 $i_o = i_3 + i_4$ ,  $i_1 + i_2 = i_o$ ,  $i_1 + i_2 = i_3 + i_4$ ,  $v_1 - v_2 - v_s = 0$ ,  
 $v_4 + v_s + v_2 - v_o = 0$ ,  $v_4 + v_s - v_3 = 0$ ,  $v_3 = v_o - v_2$ ,  
 $v_4 = v_o - v_i$ ,  $v_2 = v_i - v_s$ .

Components:  $i_1 = C_1(dv_1/dt)$ ,  $i_2 = C_2(dv_2/dt)$ ,  
 $v_3 = R_2 i_3$ ,  $v_4 = R_1 i_4$ ,  $i_s = C_s(dv_s/dt)$

Solving:

$$\frac{v_o - v_i}{R_1} = C_s \frac{dv_s}{dt} + C_1 \frac{dv_i}{dt} \quad (16)$$

$$\frac{v_o - v_2}{R_2} + C_s \frac{dv_s}{dt} = C_2 \frac{dv_2}{dt} \quad (17)$$

$$\frac{v_o - v_2}{R_2} + \frac{v_o - v_i}{R_1} = C_1 \frac{dv_i}{dt} + C_2 \frac{dv_2}{dt} \quad (18)$$

Since  $v_s = v_i - v_2$  then  $dv_s/dt = (dv_i/dt) - (dv_2/dt)$ , and so using it on equation (16), is obtained:

$$\frac{dv_2}{dt} = \left( 1 + \frac{C_1}{C_s} \right) \frac{dv_i}{dt} - \frac{v_o - v_i}{C_s R_1} \quad (19)$$

Using  $dv_s/dt = (dv_i/dt) - (dv_2/dt)$  and (19) on equation (17), is obtained:

$$v_2 = v_o + \frac{R_2(C_2 + C_s)(v_o - v_i)}{C_s R_1} + R_2 C_s \left( 1 - \left( 1 + \frac{C_2}{C_s} \right) \left( 1 + \frac{C_1}{C_s} \right) \right) \frac{dv_i}{dt} \quad (20)$$

Calculating the derivative of (20) is obtained:

$$\frac{d(v_2)}{dt} = -\frac{R_2(C_2 + C_s)}{C_s R_1} \frac{dv_i}{dt} + R_2 C_s \left( 1 - \left( 1 + \frac{C_2}{C_s} \right) \left( 1 + \frac{C_1}{C_s} \right) \right) \frac{d^2 v_i}{dt^2} \quad (21)$$

Now using (20) and (21) to remove the variables  $v_2$  and  $dv_2/dt$  from the equation (18), is obtained an equation solvable for determining  $v_i(t)$ :

$$v_o - v_i = (R_2(C_2 + C_s) + R_1(C_1 + C_s)) \frac{dv_i}{dt} + R_2 R_1 (C_1 C_2 + C_s(C_1 + C_2)) \frac{d^2 v_i}{dt^2} \quad (22)$$

The equation (22) is of the type:  $c(v_o - v_i) = b(dv_i/dt) + a(d^2 v_i/dt^2)$ , that has the general solution:

$v_i(t) = v_o + k_1 e^{\lambda_1 t} + k_2 e^{\lambda_2 t}$ , where  $k_1, k_2$  are integration constants to be defined by 'initial conditions' and  $\lambda_1, \lambda_2$  are defined by:  $a\lambda^2 + b\lambda + c = 0 \Leftrightarrow \lambda = \frac{-b \pm \sqrt{b^2 - 4ac}}{2a}$  and  $e$  is the Euler-Napier constant  $e = \sum_{n=0}^{\infty} (1/(n!))$ .

So for a solution to this circuit:  $c = 1$ ,

$$b = (R_2(C_2 + C_s) + R_1(C_1 + C_s)),$$

$$a = R_2 R_1 (C_1 C_2 + C_s(C_1 + C_2)).$$

Is selected the solution  $\lambda_2 = \frac{-b + \sqrt{b^2 - 4ac}}{2a}$  by setting  $k_1=0$ , because is the one that provides an adequate value for  $v_i(t)$ ,

$f(C_s)$ , consistent with experimental data, however for obtaining the function  $C_s(f)$  you may use any.

For convenience of making  $v_i(t)$  more similar to typical RC circuits is defined  $\tau = -1/\lambda$ , and so  $v_i(t) = v_o + k_2 e^{-t/\tau}$ .

So when is connected a capacitive sensor ( $C_s$ ) the differential equation and solution  $v_i(t)$  are the same as when is connected a resistive sensor ( $R_s$ ), the only differences are on the values of  $a, b, c$ ; and as such the equations of  $f(\text{frequency})$  and  $T(\text{period})$  are also the same and are reused from the previous section.

The constant 'H' defined by:

$$H = \ln \left( \frac{(V_T^- - V_{DDs})V_T^+}{(V_T^+ - V_{DDs})V_T^-} \right),$$

and  $f = 1/T \Leftrightarrow f = 1/(\tau_2 H) \Leftrightarrow f = -\lambda_2/H$ .

- So the expression (theoretical) of measured capacitance  $C_{sensor}$  as a function of frequency(f) is:

$$C_{sensor} = C_s = \frac{(C_1 R_1 + C_2 R_2) H f - 1 - C_1 C_2 R_1 R_2 H^2 f^2}{H f ((C_1 + C_2) R_1 R_2 H f - R_1 - R_2)} \quad (23)$$

Using the values  $C_1=C_2=2.2nF$ ,  $R_2=500\Omega$ ,  $R_1=2M\Omega$ ,  $V_T^- = 1.2V$ ,  $V_T^+ = 2.2V$ ,  $V_{DDs}=4.18V$ , is obtained  $H=1.01496$ , and Fig.17 shows the plot of  $C_s(f)$  using (23) with the mentioned values of  $C_1, C_2, R_2, R_1, H$ .

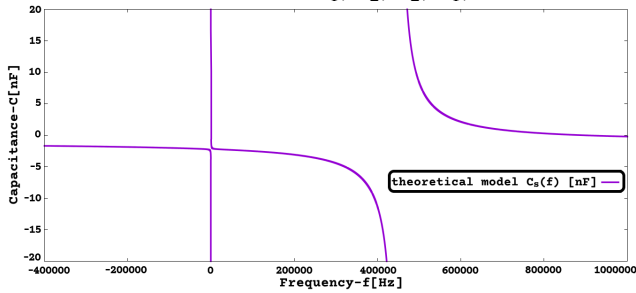


Figure 17:  $C_s(f)$  [nF] versus frequency[-400kHz, 1MHz] (Schmitt-Trigger Oscillator, Multiple-Sensor Interface with capacitive sensor).

Analyzing the plot on Fig.17 by firstly looking at plot regions with  $C_s > 0$ , its visible that the  $C_s(f)$  plot is over the vertical axis ( $f=0$ ) and this would mean that for all values of  $C_s$  the frequency would be zero ( $f=0$ ), but visible to the right is another curve that is also placed on the area of  $C_s > 0$  (for frequency[447957Hz, 895689Hz ] ) and at a first view this curve would seem appropriate. But strangely on  $C_s > 0$ ,  $f > 0$  for each value of  $C_s$  are 2 values of frequency, while for  $C_s < 0$ ,  $f > 0$  each value of  $C_s$  has only one possible value of frequency ( $f < 0$  is considered meaningless/ignored).

The experimental data shows that the way the oscillator works using a capacitive sensor is different from what some would expect on a first view of the plot  $C_s(f)$ , in order to compare the experimental data with the theoretical model is shown on Fig.18 and Fig.19 the experimental data for Multiple-Sensor Interface with various capacitance values connected as the sensor and also the plot of  $abs(C_s(f)) (= |C_s(f)|)$  using (23) with the mentioned values of  $C_1, C_2, R_1, R_2, H$ .

So it seems that the obtained function of  $C_s(f)$  although strangely indicates negative values for the sensor capacitance it can provide a theoretical curve/plot similar to what was obtained on the experimental data for  $C_{sensor}$ . On the following sections is given a better insight on why  $C_s(f)$  has a negative value.

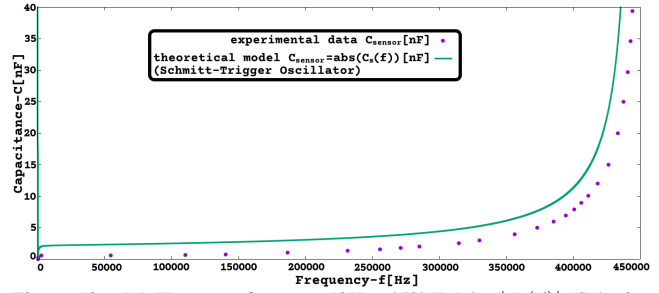


Figure 18:  $C_s$ [nF] versus frequency[0Hz, 450kHz] by  $|C_s(f)|$  (Schmitt-Trigger osc., Multi-Sensor Int. with capacitive sensor)

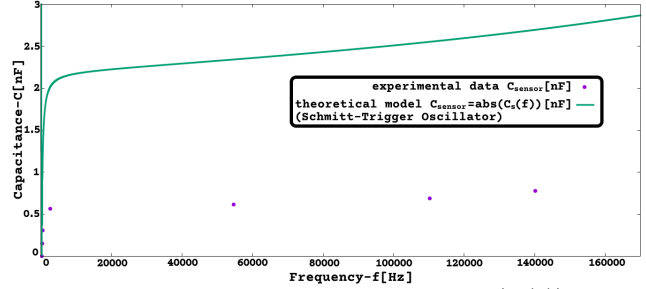


Figure 19:  $C_s$ [nF] versus frequency[0Hz, 170kHz] by  $|C_s(f)|$  (Schmitt-Trigger osc., Multi-Sensor Int. with capacitive sensor)

#### 4.4 Multiple-Sensor Int. for measuring frequency

For measuring frequency of an external voltage signal (between 0V and  $V_{DDs}$ , so preferentially a digital signal or in case of analog signal it should be limited/trimmed before) is possible to use the mentioned Multiple-Sensor Interface and so using the same port/connector of the device. For this the user should remove/open the jumpers "JPA", "JPB" making the capacitors C1-A, C2-B active on the circuit, this will make  $C_1 = C_2 = 21.8pF$  that is a quite low capacitance that will have an insignificant effect on the external voltage signal. The external voltage signal should be connected to the 1st pin of the sensor channel that is the one connected directly to input of the Schmitt-Trigger Inverter, so making the inverter directly driven by the external voltage signal, then the Multiple-Sensor Interface is just a converter of the voltage signal to a square wave signal where its frequency will be measured through the counter/timer of the PIC18F2550.

The external voltage signal would preferentially be from a sensor with a square wave output, and the sensor have its power supplied by one of the  $V_{DDs}, GND$  ports/connectors of the sensor interface device or by an external connection to the same power supply used to power the device.

### 5 Alternative Approximate Circuit Analysis

#### 5.1 Sensor interface circuit simplified

The Multiple-Sensor Interface circuit when working as Schmitt-Trigger oscillator (using  $R_s, C_s$ , or  $L_s$  with specific  $C_1, C_2$  values) can be studied and understood in a more intuitive way by making some simplification/approximation that may be inaccurate for quantitative purposes but still captures its essence, with the benefit of exposing how it works and resulting in much simpler differential equations. So the interface circuit is a more complex Schmitt-Trigger oscillator, but its essence is the same, it is just some capacitors being charged by currents that pass through some resistors, and the voltage on a capacitor ( $v_i$ ) will trigger (at  $V_T^-$  or  $V_T^+$ ) a switch (electronic inverter) to change the voltage ( $v_o$ ). (Eduardo Corpeno 2018)[3]



So the sensor and interface circuit can be described approximately as a basic Schmitt-Trigger oscillator that only has one capacitor and one resistor (that determine the frequency of oscillation), and so was used the simplified circuit on Fig.20 where  $C_{approx}$  is a capacitor and  $R_{approx}$  is a resistor that approximate in overall the capacitance and resistance of the sensor interface oscillator.

To build expressions of  $C_{approx}$  and  $R_{approx}$  that include  $R_1$ ,  $R_2$ ,  $C_1$ ,  $C_2$  are considered initially 2 extreme cases of the sensor impedance( $Z_s$ ): 1st  $|Z_s|=0$  the sensor can be replaced by a wire, and 2nd  $|Z_s|=\infty$  the sensor can be removed(open circuit), these 2 extreme cases possible for the sensor impedance are represented on Fig.21 .

Now the sensor can be described as an electric connection that can be weakened or intensified depending on the sensor impedance, so when  $|Z_s|$  changes progressively from 0 to  $+\infty$  the circuit behavior changes progressively and smoothly from the behavior of the left circuit to the behavior of right circuit of Fig.21. So to obtain equations for  $R_{approx}$  and  $C_{approx}$  was selected an expression that allows to change smoothly the resistance and capacitance of the left side circuit to the resistance and capacitance of the right side circuit of Fig.21.

So as on Fig.21, here are the values of  $C_{approx}$  and  $R_{approx}$  for the 2 extreme values of  $|Z_s|=0$  and  $|Z_s|=\infty$ :

$$\begin{aligned} C_{approx}(Z_s=0) &= C_1 + C_2; & C_{approx}(Z_s=\infty) &= C_1; \\ R_{approx}(Z_s=0) &= (R_1 R_2) / (R_1 + R_2); & R_{approx}(Z_s=\infty) &= R_1; \end{aligned}$$

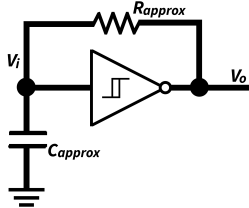


Figure 20: Schematic of a basic Schmitt-Trigger Oscillator to be used as an approximation of the circuit of Multiple-Sensor Interface.

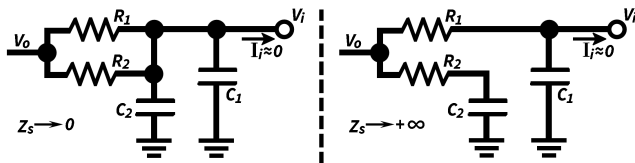


Figure 21: Schematic of the RC network of the Schmitt-Trigger Oscillator for the 2 extreme cases of the sensor impedance ( $Z_s$ ).

### 5.1.1 $R_{approx}$ and $C_{approx}$ for a resistive sensor ( $R_s$ )

Here are functions modeled to describe  $C_{approx}$  and  $R_{approx}$  (with resistive sensor) with a smooth transition from its values at  $|Z_s|=0$  and  $|Z_s|=\infty$ , where  $|Z_s|=R_s$ :

$$C_{approx} = (C_1 + C_2) \frac{R_1}{|Z_s| + R_1} + C_1 \frac{|Z_s|}{|Z_s| + R_1} \quad (24)$$

$$R_{approx} = \frac{R_1 R_2}{R_1 + R_2} \frac{2R_1}{|Z_s| + 2R_1} + R_1 \frac{|Z_s|}{|Z_s| + 2R_1} \quad (25)$$

Using the equations:  $f=1/T \Leftrightarrow f=1/(\tau H) \Leftrightarrow f=\lambda/H$ , and using  $\tau=R_{approx}C_{approx}$ , where  $|Z_s|$  was removed using  $|Z_s|=R_s$ , it can be obtained  $R_s(f)$ .

Using values  $V_T^- = 1.2V$ ,  $V_T^+ = 2.2V$ ,  $V_{DDS} = 4.18V$ , is obtained  $H = 1.01496$  (valid for any type of sensor).

Using the values  $C_1 = C_2 = 2.2nF$ ,  $R_2 = 500\Omega$ ,  $R_1 = 2M\Omega$ ,  $H = 1.01496$  with the approximate model ( $C_{approx}$ ,  $R_{approx}$ ), is obtained the plot of  $R_s(f)$  on Fig.22.

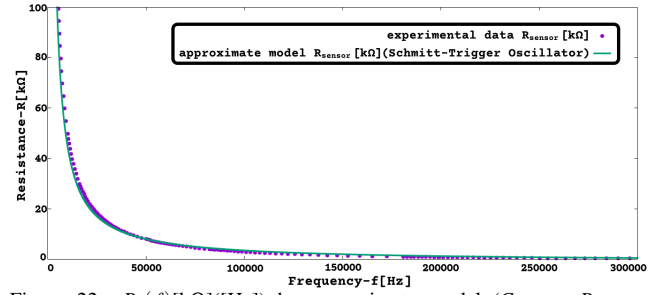


Figure 22:  $R_s(f)$ [kΩ](Hz) by approximate model ( $C_{approx}$ ,  $R_{approx}$ ; Multiple-Sensor Int. with resistive sensor).

### 5.1.2 $R_{approx}$ and $C_{approx}$ for an inductive sensor ( $L_s$ )

This approximate model for the interface circuit with inductive sensor is only valid for jumper configuration(capacitor values) that make it work as Schmitt-Trigger oscillator, as is expected for JP.A closed, JP.B open ( $C_1 = 2.2nF$ ,  $C_2 = 21.78pF$ ). Here are functions modeled to describe  $C_{approx}$  and  $R_{approx}$  (with inductive sensor) with a smooth transition from its values at  $|Z_s|=0$  and  $|Z_s|=\infty$ , where  $|Z_s|=2\pi fL_s$ :

$$C_{approx} = (C_1 + C_2) \frac{R_1}{|Z_s| + R_1} + C_1 \frac{|Z_s|}{|Z_s| + R_1} \quad (26)$$

$$R_{approx} = \frac{R_1 R_2}{R_1 + R_2} \frac{R_1}{|Z_s| + R_1} + R_1 \frac{|Z_s|}{|Z_s| + R_1} \quad (27)$$

Using the values  $C_1 = 2.2nF$ ,  $C_2 = 21.78pF$ ,  $R_2 = 500\Omega$ ,  $R_1 = 2M\Omega$ ,  $H = 1.01496$  with the approximate model ( $C_{approx}$ ,  $R_{approx}$ ), is obtained the plot of  $L_s(f)$  on Fig.23 and Fig.24.

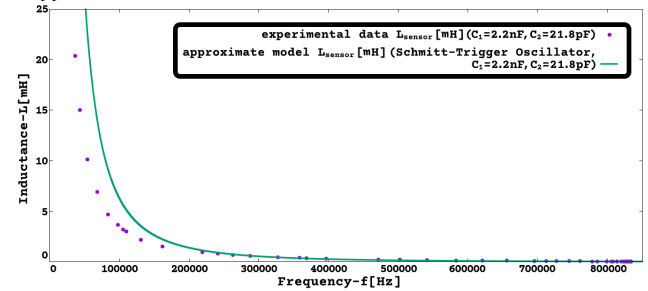


Figure 23:  $L_s$ [mH] versus frequency[0Hz, 850kHz] by approximate model ( $C_{approx}$ ,  $R_{approx}$ ; Multi-Sensor Int. with inductive sensor)

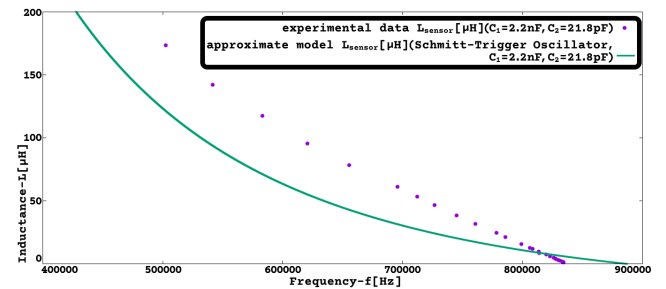


Figure 24:  $L_s$ [μH] versus frequency[400kHz, 900kHz] by approximate model ( $C_{approx}$ ,  $R_{approx}$ ; Multi-Sensor Int. with inductive sensor)

### 5.1.3 $R_{approx}$ and $C_{approx}$ for a capacitive sensor ( $C_s$ )

Here are functions modeled to describe  $C_{approx}$  and  $R_{approx}$  (with capacitive sensor) with a smooth transition from its values at  $|Z_s|=0$  and  $|Z_s|=\infty$ , where  $|Z_s|=1/(2\pi fC_s)$ :

$$C_{approx} = (C_1 + C_2) \frac{R_1}{|Z_s| + R_1} + C_1 \frac{|Z_s|}{|Z_s| + R_1} \quad (28)$$

$$R_{approx} = \frac{R_1 R_2}{R_1 + R_2} \frac{R_1}{|Z_s| + R_1} + R_1 \frac{|Z_s|}{|Z_s| + R_1} \quad (29)$$

Using the values  $C_1 = C_2 = 2.2nF$ ,  $R_2 = 500\Omega$ ,  $R_1 = 2M\Omega$ ,

$H=1.01496$ , with the approximate model ( $C_{approx}$ ,  $R_{approx}$ ), is obtained the plot  $C_s(f)$  on Fig.25 and Fig.26.

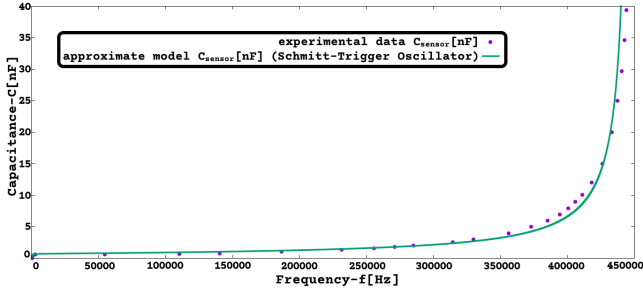


Figure 25:  $C_s$ [nF] versus frequency[0Hz, 450kHz] by approximate model ( $C_{approx}$ ,  $R_{approx}$ ; Multi-Sensor Int. with capacitive sensor)

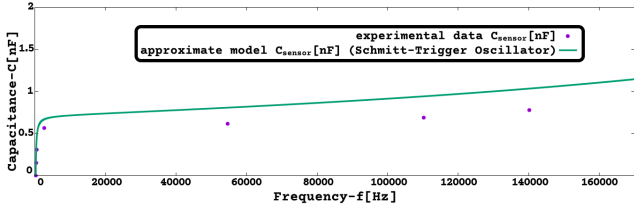


Figure 26:  $C_s$ [nF] versus frequency[0Hz, 170kHz] by approximate model ( $C_{approx}$ ,  $R_{approx}$ ; Multi-Sensor Int. with capacitive sensor)

### 5.2 Why $C_s(f) < 0$ on Multi-Sensor with capacitive sensor

About  $C_s(f) < 0$  have in mind the Multiple-Sensor with capacitive sensor is studied on transient behavior (relaxation oscillator), where 'frequency' is a measure of the speed of charge and discharge on  $C_1$ ; and also of how fast the transient circuit analysis alternates between  $v_o = V_{DDs}$  and  $v_o = 0$ .

To understand why a normal capacitor behaves as negative capacitance when connected as the sensor of the Multiple-Sensor Interface (this is, why  $C_s(f) < 0$ ), is important to highlight some things already explored on the previous sections:

1)  $C_1 = C_2$ ,  $R_1 \gg R_2$ .

2) The primary path (always available) to charge  $C_1$  is through  $R_1$ , the primary path (always available) to charge  $C_2$  is through  $R_2$ , since  $R_1 \gg R_2$  and  $C_1 = C_2$  this implies that capacitor  $C_2$  will charge/discharge much faster (takes less time) than capacitor  $C_1$ .

3) The purpose of sensor  $C_s$  on this circuit is to act as a variable impedance that can establish an alternative path on the circuit ( $V_o \rightarrow R_2 \rightarrow C_s \rightarrow C_1$ ) to charge/discharge capacitor  $C_1$ ; so  $C_s \nearrow \Rightarrow |Z_s| \searrow \Rightarrow R_{approx} \searrow \Rightarrow \tau_2 \searrow \Rightarrow C_1$  charges faster.

4) No matter how small  $|Z_s|$  may be the capacitor  $C_2$  will always charge/discharge faster than capacitor  $C_1$ , and on the limit where  $|Z_s| = 0$  the capacitors  $C_1$  and  $C_2$  will be charged/discharged simultaneously.

For the following discussion was used as definition of capacitance the formula  $C_s = i_s / (dv_s / dt)$ , where the  $|C_s| = |Q_s| / |v_s|$  ( $C_s$ : [F] farad;  $Q_s$ : [C] coulomb;  $v_s$ : [V] volt), and since the only purpose is to show how  $C_s$  can be a negative number it was used the approximate expression  $C_s \approx \bar{i}_s / (\Delta v_s / \Delta t)$  that provides exactly the same sign as the exact formula. To show is possible  $C_s < 0$  were considered qualitative relations of the circuit electrical parameters and their variation between  $t = t_1$  and  $t = t_2$  is represented on Fig.27.

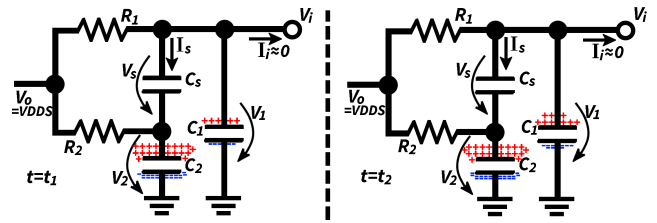


Figure 27: Schematic of RC network of the Schmitt-trigger osc. with a representation of electrical charge on  $C_1$ ,  $C_2$  at  $t = t_1$  and  $t = t_2$ .

It were assumed symbolic values for the voltages on the circuit, used as specimen values to determine how fast a voltage is changing between  $t_1$  and  $t_2$  time moments. So for representing a small amount of electrical charge are used the symbols:  $[+]$  for positive charge and  $[-]$  for negative charge, since already stated  $C_1 = C_2$  for each additional amount of  $[+]$  and  $[-]$  charge stored on each plate (of  $C_1$  or  $C_2$ ) will cause an increase of capacitor voltage that will be represented as  $[+v]$ , where  $C_1 = C_2 = [+] / [+v]$ .

As visible on Fig.27  $V_o = V_{DDs} \approx +4.18V$ , and so  $V_{DDs}$  will eventually be the voltage on  $C_1$  and  $C_2$  when  $t \rightarrow \infty$ . For making visual on the schematic the charging process, the charge accumulated in  $C_1$ ,  $C_2$  was divided in 20 sets, each represented by  $[+]$ ,  $[-]$ ; and for each set of accumulated charge is associated a corresponding increase in voltage of  $[+v]$ , and so  $[+v] = V_{DDs} / 20$ .

Accordingly on Fig.27 is represented that  $C_2$  is charged to near the final value ( $V_{DDs}$ ) during the interval  $[0; t_1]$  while  $C_1$  charges much slower. During interval  $[t_1; t_2]$  is visible that  $C_2$  increased its charge only by  $1[+]$  becoming charged to approximately (or practically) its final value ( $v_2 \approx V_{DDs}$ ), whether  $C_1$  is still charging and  $v_1$  is far from its final value ( $V_{DDs}$ ), but interestingly  $v_1$  is now increasing faster than  $v_2$ , because  $v_2$  already reached its final value, this is  $dv_1 / dt > dv_2 / dt, \forall t \in [t_1; t_2]$ . The specimen values here mentioned are in line with the exponential function typical of capacitors charging through a resistor, where lets say a capacitor initially charges very fast, when has some charge stored it charges more slowly, and when close to being full it charges very slowly (where full means the capacitor voltage is close to power supply voltage).

#### 5.2.1 Voltage and current specimens for $t = t_1$

So looking at the schematic on left side of Fig.27 is visible  $C_1$  and  $C_2$  are charging and for  $t = t_1$  the charge on  $C_1$  is  $5[+]$  and on  $C_2$  is  $19[+]$ , so capacitor  $C_2$  is almost charged while  $C_1$  is still charging. Capacitor  $C_1$  is charging through the path  $V_o \rightarrow R_1 \rightarrow C_1$  but mainly is charging through path  $V_o \rightarrow R_2 \rightarrow C_s \rightarrow C_1$ , since  $v_2 > v_1$  then  $i_s(t = t_1) < 0$ .

For  $t = t_1$ ,  $Q_1 = 5[+]$ ,  $Q_2 = 19[+]$ , then  $v_1 = 5[+v]$ ,  $v_2 = 19[+v]$ , since  $v_s = v_1 - v_2$  then  $v_s(t = t_1) = 5[+v] - 19[+v] = -14[+v]$ .

#### 5.2.2 Voltage and current specimens for $t = t_2$

So looking at the schematic on right side of Fig.27 is visible  $C_1$  and  $C_2$  are charging and for  $t = t_2$  the charge on  $C_1$  is  $9[+]$  and on  $C_2$  is  $20[+]$ , so capacitor  $C_2$  is fully charged while  $C_1$  is still charging. Capacitor  $C_1$  is charging through the path  $V_o \rightarrow R_1 \rightarrow C_1$  but mainly is charging through path  $V_o \rightarrow R_2 \rightarrow C_s \rightarrow C_1$ , since  $v_2 > v_1$  then  $i_s(t = t_2) < 0$ .

For  $t = t_2$ ,  $Q_1 = 9[+]$ ,  $Q_2 = 20[+]$ , then  $v_1 = 9[+v]$ ,  $v_2 = 20[+v]$ , since  $v_s = v_1 - v_2$  then  $v_s(t = t_2) = 9[+v] - 20[+v] = -11[+v]$ .

### 5.2.3 Sign of $C_s$ as calculated from $v_s$ and $i_s$ during $[t_1; t_2]$

The schematics on Fig.27 refer to a charging cycle of the Schmitt Trigger Oscillator. Also  $t_2 > t_1 \rightarrow \Delta t > 0$ .

For  $t \in [t_1; t_2]$  the capacitor  $C_1$  is being charged through the path  $V_o \rightarrow R_2 \rightarrow C_s \rightarrow C_1$  and so  $i_s(t) < 0, \forall t \in [t_1; t_2] \Rightarrow \bar{i}_s < 0$ . Also  $\Delta v_s$  between  $t_1$  and  $t_2$  is  $\Delta v_s = v_s(t=t_2) - v_s(t=t_1) = -11[+v] - (-14[+v]) = 3[+v]$ , so  $\Delta v_s > 0$  between  $t_1$  and  $t_2$ .

So concluding between  $t_1$  and  $t_2$ ,  $\Delta t > 0$ ,  $\Delta v_s > 0$ ,  $\bar{i}_s < 0 \Rightarrow C_s < 0$  accordingly with  $C_s \approx \bar{i}_s / (\Delta v_s / \Delta t)$ .

### 5.3 Comparison to known cases of negative capacitance

Aspects of Multiple Sensor Interface circuit possibly related to negative capacitance phenomenon:

- 1- Use of Schmitt-Trigger 'NOT' gate which exhibits hysteresis on its  $v_o(v_i)$  graph.
- 2- Multiple Sensor Interface with a capacitive sensor operates under transient(time domain) step voltage changes, caused by its 'NOT' gate(Schmitt-Trigger) alternating between 0V and +VDD5 (relaxation oscillator).

Negative capacitance phenomenon is reported on some scientific articles/texts, and interestingly with some coincidence to the 2 aspects mentioned above. Quotes:

- 1- "Effective negative capacitance has been postulated in ferroelectrics because there is hysteresis in plots of polarization-electric field.", article "Towards steep slope MOSFETs using ferroelectric negative capacitance", year 2014. (O'Neill A. 2015)[4].
- 2- "The phenomenon of negative capacitance, which has been reported in a variety of situations involving electrolytic as well as electronic systems, ... . It is suggested that the physically correct approach lies in the analysis of the corresponding time-domain behavior under step function bias, which involves a current initially falling and then rising gradually over a period of time before finally decaying to zero.", article "The physical origin of negative capacitance", year 1986. (Andrew K.Jonscher 1986) [5].

## 6 Conclusion

The author demonstrated theoretically a more versatile design for use with sensor applications, also was provided experimental data that corroborates the presented theory. The motivation of the author was to make available an electronics design that could be more sustainable in terms of life-cycle duration, by making a design more customizable by the user and also not closed/locked to a specific application/purpose. No warranty is given that the design can provide accuracy or convenience to a specific application/use; as the article is focused on showing how a versatile design can be achieved.

### Acknowledgements

I thank all of the Open-Source community for making available technology that everyone can use and build-on freely, thus inspiring me to also release this project as Open-Source. Also thanks to GNUplot software, that was used for drawing the plots on this article [13].

### Declaration of competing interest

The author declares that he has no competing interests.

## A Experimental Datasets

Here is made available subsets (small list) of experimental data with measured values of Inductance, Resistance, Capacitance paired with measured frequency on the Multiple Sensor Interface device. Is made available only a limited subset of the experimental data that was used for drawing the plots of  $L_s(f)$ ,  $R_s(f)$ ,  $C_s(f)$  for reference purposes, since placing here the full dataset would make the article exceedingly long. On the tests (Fig.28) were used arrays(PCBs) with inductor, resistor, capacitor that allow to obtain various different values just by changing a jumper/switch, also were used single components (including in series or parallel association); these fixed value components were connected as the sensor on the device.

### A.1 Frequency measurement by Multi-Sensor

- The Multiple-Sensor device measures frequency using a counter inside the microcontroller and has some accuracy and range limitations, it can measure up to 3MHz (higher frequency causes counter overflow). The Multiple-Sensor device was tested with a square wave signal from signal generator JDS6600 (by Joy-IT, frequency accuracy:  $\pm 20$ ppm).

- The Multiple-Sensor device measurement accuracy (percentage error) of frequency, is worst at low frequencies with 9% error at 100Hz and 0.7% error at 1kHz, above 5kHz the error was always smaller than 0.2% (ignoring any accuracy error by JDS6600 used as reference). The Multiple-Sensor device measurement precision (variation) for frequency was worst at low frequencies with 5% variation at 300Hz, above 1500Hz was always smaller than 1%, and above 15kHz was always smaller than 0.1%.

### A.2 Experimental data on Multi-Sensor Int.

#### - Reference instruments:

The measurements of inductance( $L_s$ ) and capacitance( $C_s$ ) were obtained using the LCR meter TH2821A (by Tonghui, basic accuracy 0.3%), configured to 10Khz test signal.

The measurements of resistance( $R_s$ ) were obtained using the meter UT603 (by UNI-T, accuracy: 0.8% for  $R \leq 2M\Omega$ ; 2% for  $R > 2M\Omega$ ).

Here are subset (some pairs) of measured experimental data for  $L_s(f)$ ,  $R_s(f)$ ,  $C_s(f)$ .

#### - Jumper Configurations:

<sup>a</sup>(JPA on, JPB off):  $C_1=2.2nF$ ;  $C_2=21.8pF$ .

<sup>b</sup>(JPA off, JPB on):  $C_1=21.8pF$ ;  $C_2=2.2nF$ .

<sup>c</sup>(JPA on, JPB on):  $C_1=2.2nF$ ;  $C_2=2.2nF$ .

- **Units:** Hz=hertz, H=henry,  $\Omega$ =ohm, F=farad.

Table 2: Subset of experimental data for  $R_s(f)$

$R_s[\Omega]$ Resistance	f[Hz] <sup>c</sup> JPA on, JPB on	$R_s[\Omega]$ Resistance	f[Hz] <sup>c</sup> JPA on, JPB on
0	456284	6970	55288
1.2	454678	9960	41879
5.2	451605	14950	29861
10.2	447385	19940	23271
20.1	439144	24900	19066
50	416407	29900	16176
99.9	383396	39800	12430
139.7	361700	49800	10091
199.5	333306	69700	7385
299	296289	99400	5320
398	268278	149300	3623
498	246214	199100	2798
697	213647	299000	1972
996	180865	498000	1284
1494	147150	697000	978
1992	125699	995000	779
2990	98819	1993000	504
3980	82153	5080000	351
4980	70593	9040000	305

Precision error(maximum frequency variation):

$\pm 1\text{kHz}$ (at low  $R_s$ );  $\pm 300\text{Hz}$ (at  $30\text{k}\Omega$ );  $\pm 100\text{Hz}$ (at high  $R_s$ )

Table 3: Subset of experimental data for  $L_s(f)$

$L_s[\mu H]$ Inductance	f[Hz] <sup>a</sup> JPA on, JPB off	f[Hz] <sup>b</sup> JPA off, JPB on	f[Hz] <sup>c</sup> JPA on, JPB on
1.21	834161	879205	446590
1.85	833014	887049	458577
4.7	826011	881239	496405
9.7	813397	858548	615743
11.77	808321	936894	1432920
15.76	799009	895932	1251070
21.39	785691	931940	1090760
31.8	760632	1056660	889633
46.7	726580	1369450	736014
53.44	712070	2853370	690970
95.34	620697	2103380	509845
173.5	502398	1575330	382571
341.8	368641	1112820	271168
558.1	287880	868105	212362
777.6	241031	737803	178480
921.2	218738	677591	163587
1491	161768	606844	124338
2171	130897	499264	102978
3170	105439	406011	84614
3640	97779	383305	79110
4646	84110	319423	69783
6880	68162	282360	57750
10140	54034	224090	47230
15040	43377	192088	38790
20375	36588	171981	33683

Precision error(maximum frequency variation):

$\pm 2\text{kHz}$  (at high 'f[Hz]');  $\pm 300\text{Hz}$  (at low 'f[Hz]');  
 $\pm 5\text{kHz}$  ( $2.85\text{MHz} \leftrightarrow 1.36\text{MHz}$ ; at <sup>b</sup> JPA off, JPB on)

Table 4: Set of experimental data for  $C_s(f)$

$C_s[\text{nF}]$ Capacitance	f[Hz] <sup>c</sup> JPA on, JPB on	$C_s[\text{nF}]$ Capacitance	f[Hz] <sup>c</sup> JPA on, JPB on
0	229	3.98	356012
0.152	321	4.97	373045
0.31	458	5.97	385032
0.568	2614	6.95	394283
0.615	54570	7.94	400750
0.689	110286	8.98	405766
0.776	140178	10.07	411246
1.015	186522	12.04	418028
1.34	231460	15.02	426040
1.58	255526	20.02	433089
1.79	271015	24.97	437446
2	285020	29.68	440382
2.56	314530	34.62	442584
2.99	329820	39.43	444235

Precision error(maximum frequency variation):

$\pm 3\text{kHz}$  ( $600\text{pF} < C_s < 1.6\text{nF}$ );  $\pm 2\text{kHz}$  ( $1.6\text{nF} < C_s < 21\text{nF}$ );  
 $\pm 1\text{kHz}$  ( $C_s > 21\text{nF}$ );  $\pm 50\text{Hz}$  ( $C_s < 600\text{pF}$ ).

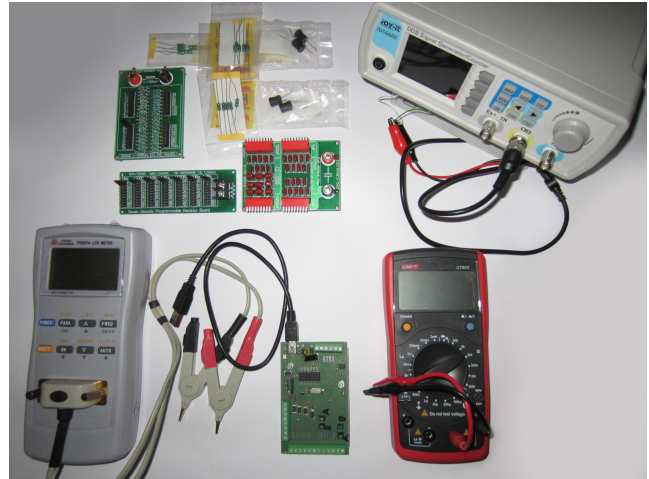


Figure 28: Equipment used for testing; R, C, L test components (top); and the Multiple-Sensor Interface (center bottom).

## References

- [1] R.C. Jaeger, T.N. Blalock (2011). Microelectronic Circuit Design (4rd ed.). McGraw-Hill. ISBN 978-0-07-338045-2. - "C.2 THE HYBRID OR h-PARAMETERS - Appendix C Two-Port Review" - Pag.1310-1311 . *Alternative Source: "Hybrid parameters (h-parameters) - Two-port Network - Wikipedia (2020)"* - [https://en.wikipedia.org/wiki/Two-port\\_network](https://en.wikipedia.org/wiki/Two-port_network)
- [2] Peter McLean (2020). Topic 4 - Crystal Oscillators (Pierce oscillator analysis) - Digital Electronics (UTS-AU). Accessed July 2021. <https://pmcl.net.au/de> .
- [3] Eduardo Corpeno - AllAboutCircuits (2018). Exactly How Schmitt Trigger Oscillators Work. Accessed July 2021. <https://www.allaboutcircuits.com/technical-articles/exactly-how-schmitt-trigger-oscillators-work> .
- [4] A. O'Neill, D. Appleby, N. Ponon, K. Kwa (2015). Towards steep slope MOSFETs using ferroelectric negative capacitance. 2014 12th IEEE International Confer-

- ence on Solid-State and Integrated Circuit Technology (ICSICT). DOI: 10.1109/ICSICT.2014.7021281 .
- [5] Andrew K. Jonscher (1986). The physical origin of negative capacitance. *J. Chem. Soc., Faraday Trans. 2*, vol. 82, no. 1, Pag.75-81. DOI: 10.1039/F29868200075 .
- [6] S. N. Nihtianov, G. P. Shterev, B. Iliev and G. C. M. Meijer, (2001), An interface circuit for R-C impedance sensors with a relaxation oscillator. *IEEE Transactions on Instrumentation and Measurement*, vol. 50, no. 6, Pag. 1563-1567, DOI: 10.1109/19.982945 .
- [7] J. H. Lu, M. Inerowicz, S. Joo, J. Kwon and B. Jung, (2011), A Low-Power, Wide-Dynamic-Range Semi-Digital Universal Sensor Readout Circuit Using Pulsewidth Modulation. *IEEE Sensors Journal*, vol. 11, no. 5, Pag. 1134-1144. DOI: 10.1109/JSEN.2010.2085430 .
- [8] F.M.L.v.d. Goes, G.C.M. Meijer, (1997). A Universal Transducer Interface for Capacitive and Resistive Sensor Elements. *Analog Integrated Circuits and Signal Processing* 14, Pag. 249–260. DOI: 10.1023/A:1008246103915 .
- [9] Xiaowen Liu, D. Rairigh, Chao Yang and A. J. Mason, (2009) Impedance-to-digital converter for sensor array microsystems, 2009 IEEE International Symposium on Circuits and Systems (ISCAS), Pag. 353-356, DOI: 10.1109/ISCAS.2009.5117758 .
- [10] Dumbrava V., Svilainis L. (2007). The Automated Complex Impedance Measurement System. *Elektronika Ir Elektrotechnika*, 76(4), Pag. 59-62. <https://eejournal.ktu.lt/index.php/elt/article/view/10720>
- [11] HIOKI website (2021), LCR meter basic measurement principles. Accessed December 2021. [https://www.hioki.com/global/learning/usage/lcr-meters\\_1.html](https://www.hioki.com/global/learning/usage/lcr-meters_1.html) .
- [12] Bi H., Yin K., Xie X., Ji J., Wan S., Sun L., Terrones M., Dresselhaus M. S., (2013). Ultrahigh humidity sensitivity of graphene oxide. *Sci Rep.* 2013;3:2714. DOI: 10.1038/srep02714 .
- [13] Thomas Williams, Colin Kelley (2007) - GNU-plot software. Accessed July 2021. <http://gnuplot.sourceforge.net> .